

Research article

Han Li, Jiajun Wang, Yating Ma, Jiao Chu, Xiang'ai Cheng, Lei Shi* and Tian Jiang*

Enhanced directional emission of monolayer tungsten disulfide (WS_2) with robust linear polarization via one-dimensional photonic crystal (PhC) slab

<https://doi.org/10.1515/nanoph-2020-0294>

Received May 18, 2020; accepted July 14, 2020; published online July 28, 2020

Abstract

Objectives: Monolayer transition metal dichalcogenides (TMDCs) have been regarded as promising candidates for the future light-emitting devices. To date, though the modulation of emission intensity and directionality in monolayer TMDCs has received considerable scholarly attention, there has been no systematic investigation on the underlying critical polarization. The intensity, directionality and robust polarization are highly favorable and pivotal for the future on-chip optoelectronic emission devices based on TMDCs.

Methods: We explore the emission features of the monolayer TMDCs in the photonic crystal (PhC) platform at room temperature. A monolayer tungsten disulfide (WS_2) is specifically integrated with a tailored PhC structure. Angle-resolved photoluminescence (PL), time-resolved PL and

polarized PL measurements are carried out to study the enhanced emission and polarization properties.

Results: The photoluminescence (PL) of WS_2 is greatly enhanced by over 300-fold, resulting from a ~fivefold enhancement (from 1.5 to 7.2%) of the PL efficiency with accelerated spontaneous emission rates. Additionally, the overall polarized emission is obtained with the degree of linear polarization (DLP) up to 60%, which is independent of the excitation polarization. Moreover, two branched directional emissions with horizontal polarization are also achieved at a divergency angle of only 3.5° , accompanied by a surprising near-100% DLP at $\pm 8^\circ$ directions.

Conclusions: This comprehensive study sets out to assess the feasibility of the high-performance light emission device based on the monolayer TMDCs and PhC structures.

Keywords: directionality; PL enhancement; polarization; WS_2 .

1 Introduction

In the last two decades, there has been a surge of research interest in exploring the low-cost, energy-efficient, scalable and environment-friendly active materials, which are critical components for optoelectronic emission devices [1–5]. Recently, monolayer transition metal dichalcogenides (TMDCs), such as tungsten disulfide (WS_2) and molybdenum disulfide (MoS_2), have emerged as significant direct-bandgap semiconductors in the visible range [6–11]. With the quantum efficiency superior to the traditional optoelectronic materials like gallium arsenide, indium phosphide and silicon, monolayer TMDCs are viewed as one of the most promising candidates for future light-emitting platforms [12, 13]. However, the quantum yield of untreated monolayer TMDCs turns to be rather low (typically less than 1%) at room temperature, resulting in a weak photoluminescence (PL) behavior [8, 14, 15]. Various approaches have been developed and introduced to reinforce the

Han Li and Jiajun Wang: These authors contributed equally to this work.

***Corresponding authors: Lei Shi,** State Key Laboratory of Surface Physics, Key Laboratory of Micro- and Nano-Photonics Structures (Ministry of Education), Department of Physics, Fudan University, Shanghai, 200433, China, E-mail: lshi@fudan.edu.cn; and **Tian Jiang,** College of Advanced Interdisciplinary Studies, National University of Defense Technology, Changsha, 410073, China, E-mail: tjjiang@nudt.edu.cn. <https://orcid.org/0000-0003-3343-5548> (T. Jiang)

Han Li, Yating Ma and Xiang'ai Cheng: College of Advanced Interdisciplinary Studies, National University of Defense Technology, Changsha, 410073, China, E-mail: kadurjie@163.com (H. Li), yating_martina@163.com (Y. Ma), 1874620361@qq.com (X. Cheng)
Jiajun Wang and Jiao Chu: State Key Laboratory of Surface Physics, Key Laboratory of Micro- and Nano-Photonics Structures (Ministry of Education), Department of Physics, Fudan University, Shanghai, 200433, China, E-mail: jjwang19@fudan.edu.cn (J. Wang), jchu18@fudan.edu.cn (J. Chu)

emission of monolayer TMDCs, including integration of noble metal nanoantenna via localized surface plasmon [16–24], chemical modification [14, 25] and construction of heterostructures with additional high-absorption perovskite materials [26, 27]. While some improvements have been observed, there are some realistic limitations using these methods. More specifically, in addition to intrinsic optical losses and high cost, precisely controlled contact is necessary during integrating noble metal nanostructures with TMDCs; otherwise, PL quenching is likely to occur instead of PL enhancement. Additionally, chemical modification suffers from undesired residual and defects, whereas the stability and toxicity of TMDCs/perovskite heterostructures under ambient conditions remain a giant challenge. These limitations would hinder the practical applications of monolayer TMDCs in on-chip emission devices. Besides, the directionality and robust polarization are also important factors determining the performance of future on-chip optoelectronic emission devices [5, 15, 28, 29]. Unfortunately, monolayer TMDCs usually exhibit poor emission polarization at room temperature [30–34]. Although the atomically thin MoS₂ nanocrystals (~nm) are reported to have 60% linear-polarized PL owing to locally unitive configuration of crystallographic axes at cryogenic conditions, the PL linear polarization degree is rapidly suppressed with lifted temperature [35]. Therefore, it is highly urgent and desired to find an approach that can enhance both the directional emission intensity and robust polarization of monolayer TMDCs, in order to promote the practical applications of on-chip devices based on monolayer TMDCs.

Photonic crystals (PhCs) are optical structures consisting of periodic nanopatterns. Benefiting from their tunable optical band structures and compatibility with the current semiconductor processing technology, PhCs are regarded as one of the most successful researched routes toward high-performance optoelectronic devices based on monolayer TMDCs. The integration of PhC with monolayer TMDCs furnishes an ideal platform to explore the underlying new physics and functionalities, such as strong light-matter interaction [36–39], photon guiding [40], emission enhancement [5, 15, 41, 42] and nanolasers [43, 44]. Polarization modulation is one of these interesting and intriguing features of PhCs that can assist TMDCs with polarized emission [45, 46]. Though considerate efforts have been spent on the modulation of emission intensity and directionality in monolayer TMDCs with PhC, the underlying critical polarization property is rarely explored. Thus, it is of significant importance to take the emission intensity, directionality and robust polarization as a whole into consideration when characterizing the TMDCs/PhC structures.

In this work, we present a comprehensive study on the emission features of monolayer WS₂ modulated by PhC slab at room temperature. We utilize a monolayer WS₂ membrane supported by PhC slab to form an emission device, as shown in Figure 1. The band structure of PhC slab is specially designed to overlap the PL spectrum of WS₂, leading to PL intensity greatly enhanced by over 300 times compared to WS₂ on flat slab. The time-resolved PL (TR-PL) decay measurements reveal that the spontaneous emission rate of WS₂ membrane is lifted after the integration with PhC slab, accompanied by ~fivefold increment of radiative recombination ratio. Moreover, the robust polarized emission is achieved with 60% degree of linear polarization (DLP) in WS₂ membrane on the PhC slab at room temperature, showing no dependence on the excitation polarization. Especially, angle-resolved PL measurements show that a robust near-100% DLP of WS₂ membrane on the PhC slab is obtained at a directional emission angle of ±8°. Within this framework of integrating PhC slab with a designed band structure, effective emission with robust polarization can be tailored by replacing other TMDC media in various applications. Our work helps in designing future on-chip optoelectronic emission devices with robust onefold polarization.

2 Results and discussion

The monolayer WS₂/PhC device is prepared by transferring a chemical vapor deposition (CVD)-grown monolayer WS₂ membrane onto the prefabricated PhC slab via a dry-transfer method. More detailed description about device preparation is provided in Methods section. The schematic of monolayer WS₂/PhC device is illustrated in Figure 1a. The in-plane electric field component parallel (perpendicular) to the grating trenches refers to the horizontal or H (vertical or V) polarization according to lab orientation. Figure 1b shows the optical band structure in Γ -X direction of the PhC slab with selected parameters, which is simulated by the finite element method with COMSOL Multiphysics software. There are two different optical bands overlapping the PL spectrum of WS₂, namely, band 1 and band 2. The simulated electric field distribution is illustrated in Figure 1c, showing band 1 is TE-like mode with the electric field mainly in the XOZ plane and band 2 is TM-like mode with electric field mainly along Z axis. Moreover, the electric field of band 1 is confined in the surface of the Si₃N₄/SiO₂ layer, which indeed overlaps with the WS₂ monolayer placed on top, while the electric field of band 2 is confined in the surface of the Ag film. Therefore, only the optical mode of band 1

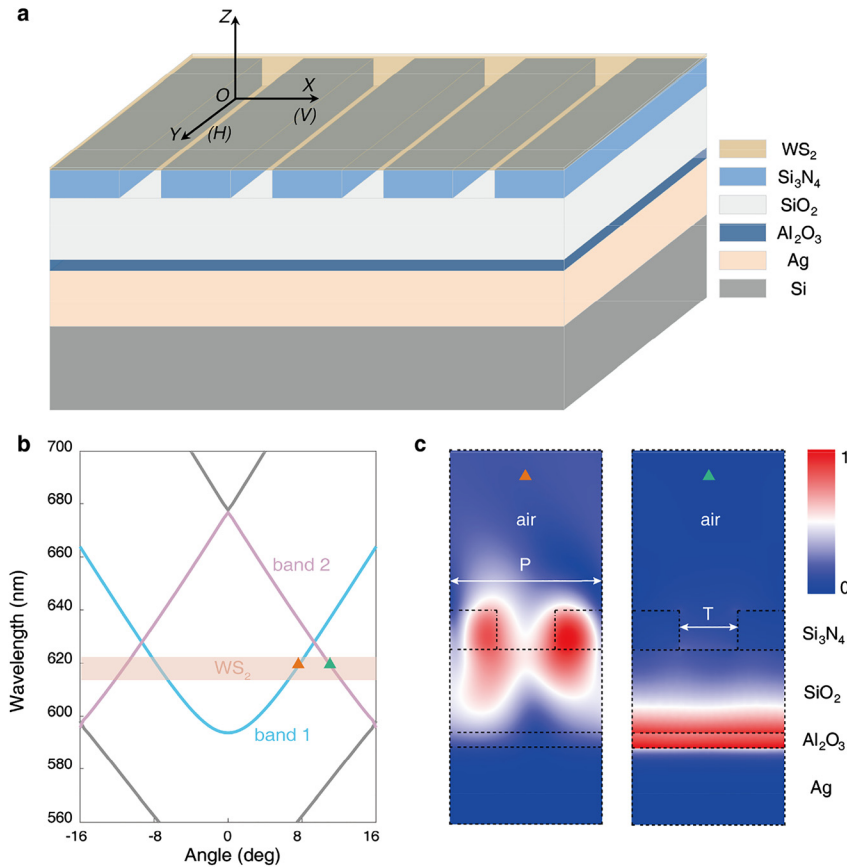


Figure 1: Schematic of the monolayer WS_2 /PhC device and simulation results.

(a) Schematic of the monolayer WS_2 /PhC device. Notably, the in-plane electric field component in along-bar (across-bar) direction of the grating corresponds to the horizontal or H (vertical or V) polarization during measurements, according to lab orientation. (b) Simulated optical band structure along Γ -X direction. Two bands, denoted as band 1 and band 2, cross the monolayer WS_2 band (marked with a salmon-pink belt), with the intersection from band 1 (band 2) marked by an orange (green) triangle. (c) Simulated electric field distribution at intersections from (b) in the XOZ plane. The simulated results are shown in a unit of the PhC slab, with finer structure components marked by dashed lines. The period (P) and trench width (T) of grating are 400 and 150 nm. The layers' thickness: Si_3N_4 , 100 nm; SiO_2 , 220 nm; Al_2O_3 , 40 nm; Ag, 200 nm; WS_2 , tungsten disulfide; PhC, photonic crystal.

interacts with the excitonic mode of monolayer WS_2 , which will be further proved in later discussion.

The PhC slab is fabricated with electron-beam lithography and reactive ion etching (RIE; for more details, see Materials and methods). We first focus on band 1 of PhC slab, and the angle-resolved measurements are performed, presented in Figure 2. Figure 2a is the reflectance of the PhC slab detected in horizontal polarization, indicating that the radiative field of band 1 is horizontal polarized. Result of vertical polarization is presented in Figure S3 of Supporting material, showing vertically polarized band 2. The WS_2 monolayer is then transferred onto the PhC slab (see Materials and methods). And the angle-resolved spectrum is measured after integrating PhC slab with monolayer WS_2 membrane in Figure 2b, showing an inconspicuous WS_2 band of exciton resonance. The darkened part of reflectance spectrum at the intersections between band 1 and WS_2 exciton resonance means an enhanced absorption, indicating an efficient contact in the monolayer WS_2 /PhC device. Additionally, the effective coupling is further identified by measuring the emission behavior in the device.

2.1 Giant PL enhancement from the WS_2 /PhC device

PL spectra are measured to assess the emission behavior at room temperature. It is found from Figure 3a that a giant PL enhancement (over 300 times) is achieved in the monolayer WS_2 /PhC device, associated with a slight blue shift behavior due to the partly suspension when compared with the monolayer WS_2 on flat slab. Besides, the giant emission enhancement also yields the successful integration of monolayer WS_2 with the PhC slab. To gain additional insights into the enhanced emission characteristics, we carry out TR-PL measurements for dynamical analysis according to obtained PL spectra. We notice that the dynamics of monolayer WS_2 in the device is largely modified. And two contrasting dynamics are recorded and fitted with a biexponential recombination model, as shown in Figure 3b. In a typical normalized biexponential model, carriers are supposed to recombine via the nonradiative and radiative processes, resulting in a TR-PL signal. When the time delay of signal rising edge is ignored, TR-PL decay is mathematically expressed as

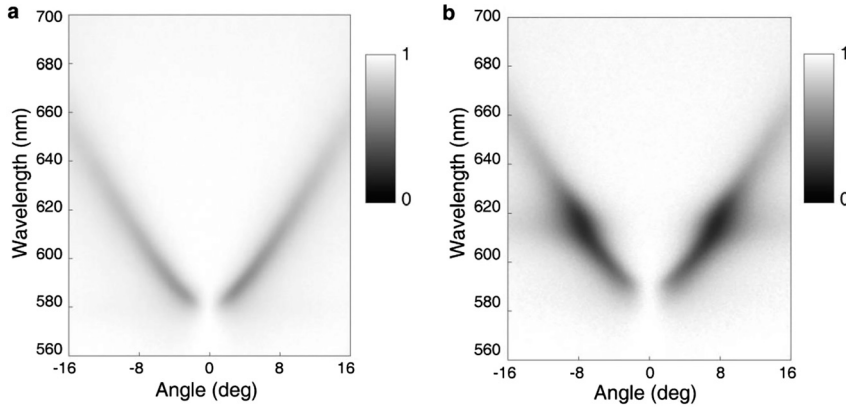


Figure 2: Measured angle-resolved reflectance spectra. (a) Reflectance spectrum for PhC slab. (b) Reflectance spectrum for the monolayer WS₂/PhC structure. The spectra are measured along Γ -X direction. WS₂, tungsten disulfide; PhC, photonic crystal.

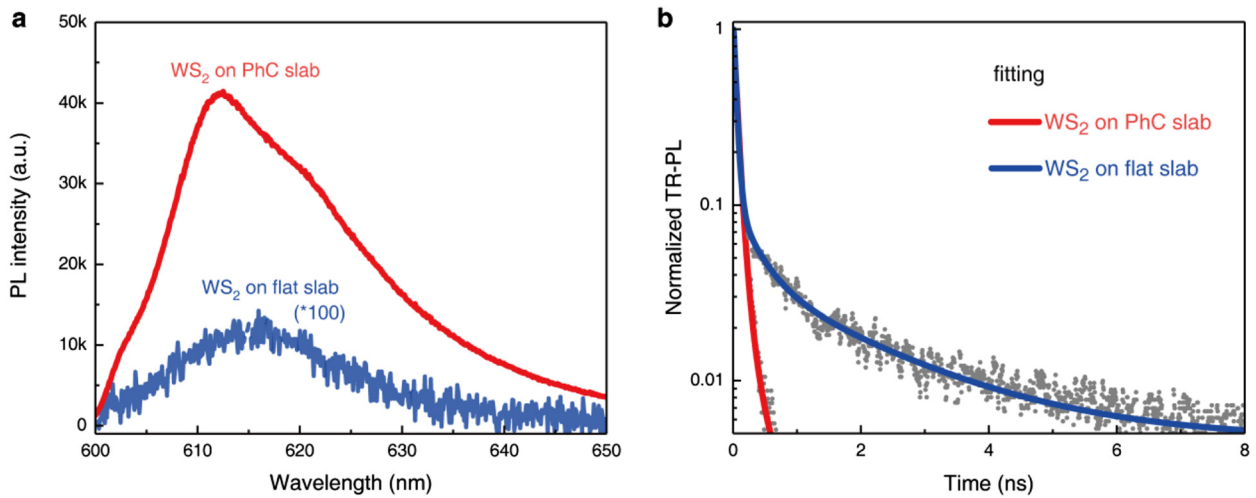


Figure 3: PL spectra and TR-PL decays.

(a) Giant PL enhancement (>300 times) in the monolayer WS₂/PhC device. PL intensity of monolayer WS₂ on flat slab is amplified for clear comparison. (b) Normalized TR-PL traces of monolayer WS₂ on PhC and flat slab in log scale. Gray curves: measured TR-PL data; red and blue curves: fitting results with the biexponential model. PL, photoluminescence; TR-PL, time-resolved PL; WS₂, tungsten disulfide; PhC, photonic crystal.

$$I(t) = A \cdot e^{-\frac{t}{\tau_1}} + (1 - A) \cdot e^{-\frac{t}{\tau_2}} \quad (1)$$

where A ($1-A$) and τ_1 (τ_2) represent the ratio and lifetime of modeled nonradiative (radiative) process, respectively. Detailed TR-PL fitting results are provided in Table S1 of Supporting material, and here, we focus on corresponding differences in dynamics. When integrated onto the PhC slab, the PL efficiency (radiative recombination ratio) of monolayer WS₂ largely increases by ~fivefold, from initial 1.5% on flat slab to 7.2% in the device. The enhanced PL efficiency indicates restrained doping and nonradiative process assisted by defects and traps [15]. Besides the altered recombination ratios, corresponding recombination rate, namely, the reciprocal of lifetime, is also accelerated. Benefitting from both spectral and spatial overlap with the optical mode from the PhC slab, available local density of photonic states during WS₂ emission increases,

resulting in a much faster spontaneous emission (radiative) rate of WS₂. And in contrast, it is worth noticing that the nonradiative recombination rate in WS₂ almost remains unchanged after integration with the PhC slab (see Table S1 of Supporting material). In this way, the overall quantum efficiency of WS₂ is then effectively improved [15, 42]. In general, TR-PL results reveal that both lifted PL efficiency and spontaneous emission rate contribute to successful PL enhancement in the monolayer WS₂/PhC slab device.

2.2 Robust linear-polarized emission of the WS₂/PhC device

Now, we consider the overall polarization property that is extremely crucial for future on-chip applications of WS₂/PhC device. Here, a dimensionless factor is proposed to

characterize the linear polarization emission property, which is expressed as

$$DLP = \frac{I_H - I_V}{I_H + I_V} \quad (2)$$

where I_H (I_V) represents the PL component detected in horizontal (vertical) polarization when pumped by a linear-polarized light source. The monolayer WS₂ on flat slab shows a neglectable linear polarization behavior, as indicated in Figure S4 of Supporting material, which has also been discussed in an early report [33]. In contrast, an obvious linear-polarized emission is discovered with a maximum DLP of 60% around 625 nm at room temperature. By switching the excitation laser from horizontal

polarization to vertical polarization, a fairly similar robust polarization behavior is reproduced and observed, as presented in Figure 4. In order to characterize the linear-polarized emission behavior from the device, polarization-resolved emission intensity at 625 nm, which is of the upmost DLP, is measured with various rotated detection angles (0–360°) under orthogonal excitation polarizations. The normalized PL intensities under these conditions are demonstrated in Figure 4c and 4d. For monolayer WS₂ on flat slab, the polarization behavior is nearly indiscernible with rather small DLP (within 2%). In this way, the orientation of emitted polarization in monolayer WS₂ is almost undistinguishable. However, the polarization orientation emitted from the WS₂/PhC device is distinct and

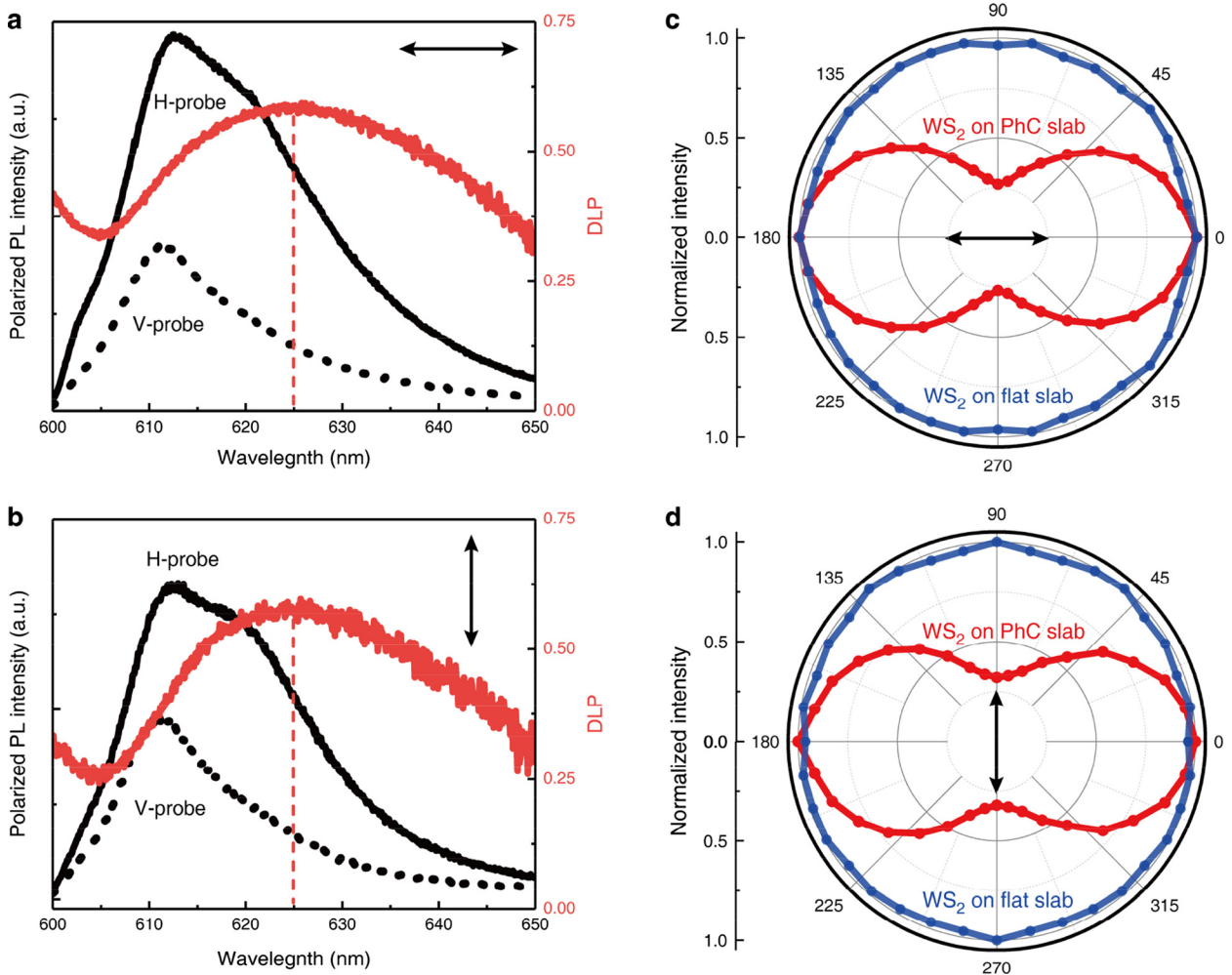


Figure 4: Polarization-resolved PL spectra.

(a–b) Linear polarization-resolved spectra of the monolayer WS₂/PhC device. Red dashed lines indicate upmost 60% linear polarization degree at 625 nm. (c–d) Normalized PL intensity from monolayer WS₂ on PhC and flat slab at 625 nm with detection angle. The orientations of black arrow represent applied excitation with horizontal polarization in (a) and (c) and vertical polarization in (b) and (d), respectively. WS₂, tungsten disulfide; PhC, photonic crystal; DLP, degree of linear polarization.

surprisingly robust, which maintains horizontal polarization and is insensitive to excitation. In fact, the observed single horizontal polarization is primarily caused by the optical mode of the PhC slab, as discussed previously. Once integrated with the PhC slab, far-field emission polarization of monolayer WS₂ is largely modified into the robust horizontal polarization, which then no more follows the excitation.

2.3 Near-100% polarization in angle-resolved PL

To further study the distribution of polarized emission in the far field, the angle-resolved PL measurements are

conducted, revealing the underlying angular information under a linear-polarized laser excitation, as illustrated in Figure 5a and 5b. It is clearly shown that the PL of horizontal polarization is notably enhanced at symmetric regions of radiative angle, meaning the emission is directional in the far field. In contrast, the PL of vertical polarization is low intensity and exhibits no directionality. All these results prove that only the optical mode of band 1 from the PhC slab interacts with the excitonic mode of monolayer WS₂, consistent with the previous deduction. Moreover, we extract the angular PL intensity in the two orthogonal directions at 625 nm for subtle polarization analysis in Figure 5c. And there are two branched directional emissions in horizontal polarization clearly observed with only 3.5° divergency angle. Meanwhile, a

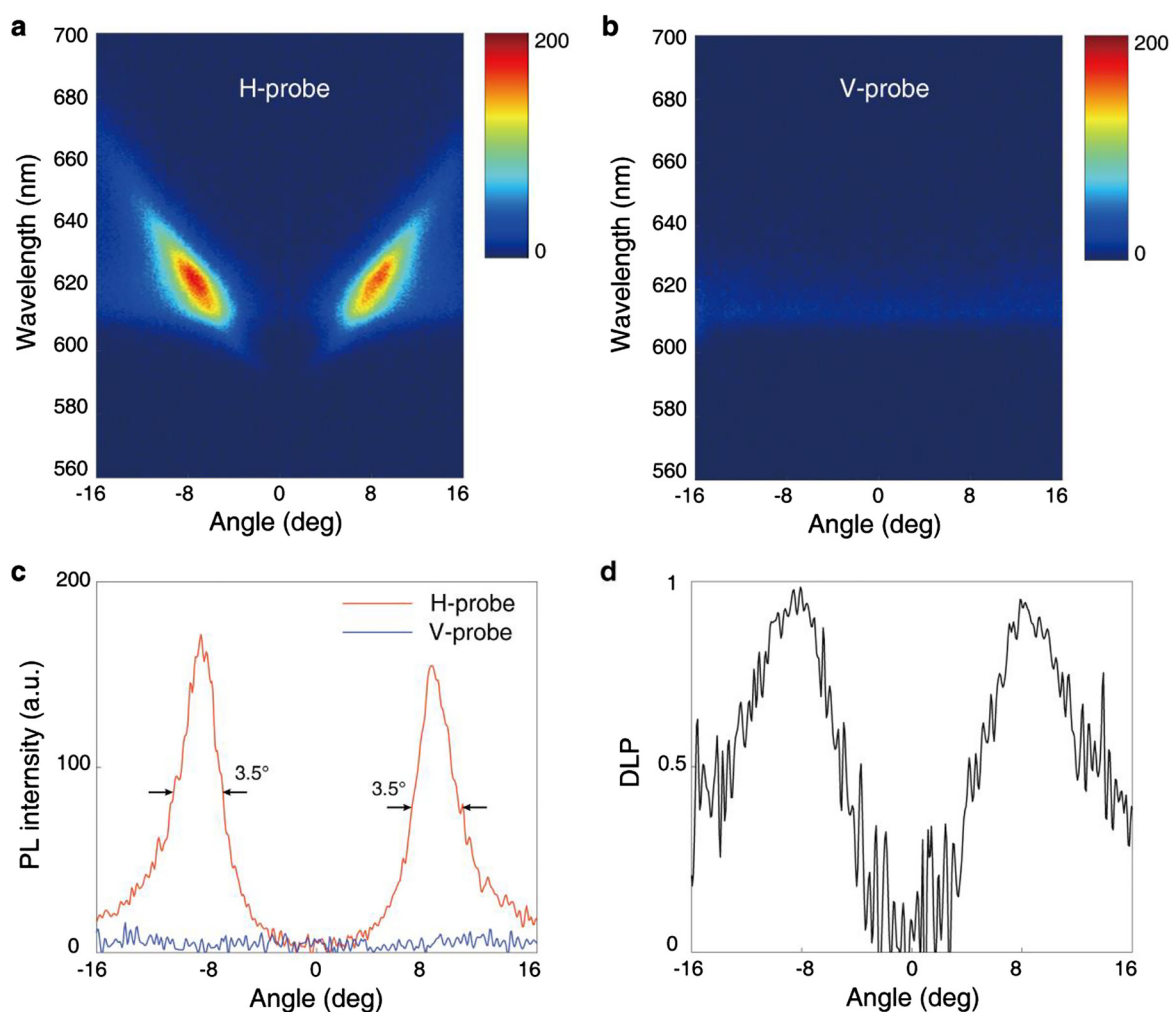


Figure 5: Angle-resolved PL spectra.

(a–b) Angle-resolved PL spectra of the monolayer WS₂/PhC device, probed in (a) horizontal and (b) vertical polarization. (c) Angle-resolved PL intensity at 625 nm in horizontal (red) and vertical polarization (blue). (d) Angle-resolved DLP, extracted from (c). An emission of robust near-unity DLP is obtained at a directional angle of $\pm 8^\circ$ from the device. PL, photoluminescence; DLP, degree of linear polarization; WS₂, tungsten disulfide; PhC, photonic crystal.

surprising near-100% DLP emission is achieved at the directional angle of $\pm 8^\circ$ in Figure 5d, which matches well with the intersections of TE-like mode and WS₂ exciton band. It is important to stress that in all angle-resolved PL measurements, the excitation laser is specifically set to 45° linear polarization, which means the equivalent components of the horizontal and vertical polarization. Even under excitation with vertical polarization component, the monolayer WS₂/PhC device still exhibits an emission of robust directionality and polarization, which is very beneficial to the next-generation on-chip polarization-related applications.

3 Conclusion

In summary, we have established an in-depth investigation on the emission features of monolayer TMDCs/PhC device at room temperature. The angle-resolved PL measurements are conducted in order to fully characterize emission intensity, directionality and robust polarization of the new device. Our comprehensive results reveal that the PL of WS₂ on the PhC slab is greatly enlarged by over 300 times. Moreover, the spontaneous emission rate of monolayer WS₂ as well as corresponding radiative recombination ratio is both boosted by integrating the monolayer WS₂ with the PhC slab. Additionally, the robust polarized emission in monolayer WS₂ on the PhC slab is discovered with up to 60% linear polarization, which is irrelevant with the excitation polarization. Finally, a robust near-100% DLP of WS₂ on the PhC slab is obtained at a directional emission angle of $\pm 8^\circ$. This work has not only examined the factors which are believed to determine the TMDC-based devices with efficient emission and robust polarization but also confirmed the feasibility of tailoring these emission characteristics by integrating potential active media in various PhC-based structures.

4 Materials and methods

4.1 Fabrication of the PhC slab

The PhC structure consists of multiple layers of slab on the Si substrate, with a thin etched Si₃N₄ layer on the top. The 200-nm-thick Ag layer and 40-nm-thick Al₂O₃ layer are grown on the Si substrate by magnetron sputtering deposition. Then the 220-nm-thick silicon dioxide layer and 100-nm-thick silicon nitride layer are grown by plasma-enhanced chemical vapor deposition. To fabricate the designed structure, the prefabricated structure is spin-coated with a layer of positive electron beam resist (PMMA950K A4) and an additional layer of conductive polymer (AR-PC 5090.02). Then, electron-

beam lithography (ZEISS, Germany, ZEISS sigma 300) is used for mask pattern onto the PMMA layer. Anisotropic etching in the silicon nitride layer is carried out by RIE with CHF₃ and O₂. Finally, patterned PMMA layer is removed by RIE using O₂ before transfer of monolayer WS₂ membrane.

4.2 Transfer of monolayer WS₂ membrane onto the PhC slab

CVD-grown monolayer WS₂ membrane on sapphire substrate is spin-coated with poly (L-lactic acid) (PLLA), followed by 75 °C baking for 5 min. Afterward, a polydimethylsiloxane (PDMS) elastomer is placed on PLLA film and tear off. In this way, the WS₂ membrane supported by PDMS with PLLA in between is obtained, which is then attached to a glass slide under the microscope on a transfer stage with the prefabricated grating underneath. With the help of a microscope, the glass slide with monolayer WS₂ membrane is lowered to contact the grating, while the transfer stage is heated to 75 °C for 2 min and cooled to room temperature. Afterward, the glass slide is lifted with PDMS on it, leaving WS₂ membrane on the grating, which is then dissolved in dichloromethane, and PLLA is removed.

4.3 Optical measurements

Angle-resolved reflectance and PL measurements are done by a lab-built system, with excitation light of 532-nm continuous-wave laser. And for polarization-resolved PL measurements, a half-wave plate and a polarizer with horizontal polarization are set in front of the spectrometer. The detection angle is controlled by rotating the half-wave plate. For TR-PL measurements, a 400-nm laser (100 fs, 80 MHz), obtained by second-harmonic generation of 800-nm fs laser with a β -BaB₂O₄ (BBO) crystal, is utilized for excitation. And TR-PL decay traces are recorded with a time-correlated single-photon counting device.

Acknowledgments: The authors are grateful for financial support from National Natural Science Foundation (NSF) of China (11802339, 11805276, 61805282, 61801498, 11804387, 11902358, 11774063, 11727811 and 91750102); the Scientific Researches Foundation of National University of Defense Technology (ZK16-03-59, ZK18-01-03, ZK18-03-36, ZK18-03-22); the NSF of Hunan province (2016JJ1021); Hunan Provincial Innovation Foundation for Postgraduate (CX2018B006); the Open Research Fund of Hunan Provincial Key Laboratory of High Energy Technology (GNJGJS03); the Opening Foundation of State Key Laboratory of Laser Interaction with Matter (SKLLIM1702) and The Youth talent lifting project (17-JCJQ-QT-004). This work is also supported by China National Key Basic Research Program (2016YFA0301103, 2016YFA0302000 and 2018YFA0306201) and Science and Technology Commission of Shanghai Municipality (19XD1434600, 2019SHZDZX01, 19DZ2253000).

Author contributions: All the authors have accepted responsibility for the entire content of this submitted manuscript and approved its submission.

Research funding: The authors are grateful for financial support from National Natural Science Foundation (NSF) of China (11802339, 11805276, 61805282, 61801498, 11804387, 11902358, 11774063, 11727811 and 91750102); the Scientific Researches Foundation of National University of Defense Technology (ZK16-03-59, ZK18-01-03, ZK18-03-36, ZK18-03-22); the NSF of Hunan province (2016JJ1021); Hunan Provincial Innovation Foundation for Postgraduate (CX2018B006); the Open Research Fund of Hunan Provincial Key Laboratory of High Energy Technology (GNJGJS03); the Opening Foundation of State Key Laboratory of Laser Interaction with Matter (SKLLIM1702) and The Youth talent lifting project (17-JCJQ-QT-004). This work is also supported by China National Key Basic Research Program (2016YFA0301103, 2016YFA0302000 and 2018YFA0306201) and Science and Technology Commission of Shanghai Municipality (19XD1434600, 2019SHZDZX01, 19DZ2253000).

Competing interests: Authors state no conflicts of interest.

References

- [1] A. K. Geim and I. V. Grigorieva, “Van der Waals heterostructures,” *Nature*, vol. 499, pp. 419–425, 2013.
- [2] K. S. Novoselov, A. Mishchenko, A. Carvalho, et al., “2D materials and van der Waals heterostructures,” *Science*, vol. 353, 2016, aac9439, <https://doi.org/10.1126/science.aac9439>.
- [3] S. Z. Butler, S. M. Hollen, L. Cao, et al., “Progress, challenges, and opportunities in two-dimensional materials beyond graphene,” *ACS Nano*, vol. 7, pp. 2898–2926, 2013.
- [4] D. Liang and J. E. Bowers, “Recent progress in lasers on silicon,” *Nat. Photonics*, vol. 4, pp. 511–517, 2010.
- [5] C.-H. Liu, G. Clark, T. Fryett, et al., “Nanocavity integrated van der Waals Heterostructure light-emitting tunneling diode,” *Nano Lett.*, vol. 17, pp. 200–205, 2017.
- [6] Q. H. Wang, K. Kalantar-Zadeh, A. Kis, et al., “Electronics and optoelectronics of two-dimensional transition metal dichalcogenides,” *Nat. Nanotechnol.*, vol. 7, pp. 699–712, 2012.
- [7] S. W. Han, H. Kwon, S. K. Kim, et al., “Band-gap transition induced by interlayer van der Waals interaction in MoS₂,” *Phys. Rev. B*, vol. 84, 2011, Art no. 45409.
- [8] K. F. Mak, “Atomically thin MoS₂ a new direct-gap semiconductor,” *Phys. Rev. Lett.*, vol. 105, 2010, Art no. 136805.
- [9] E. S. Kadantsev and P. Hawrylak, “Electronic structure of a single MoS₂ monolayer,” *Solid State Commun.*, vol. 152, pp. 909–913, 2012.
- [10] K. Wei, Y. Liu, H. Yang, et al., “Large range modification of exciton species in monolayer WS₂,” *Appl. Opt.*, vol. 55, p. 6251, 2016.
- [11] H. Li, X. Zheng, Y. Liu, et al., “Ultrafast interfacial energy transfer and interlayer excitons in the monolayer WS₂/CsPbBr₃ quantum dot heterostructure,” *Nanoscale*, vol. 10, pp. 1650–1659, 2018.
- [12] O. Salehzadeh, N. H. Tran, X. Liu, et al., “Exciton kinetics, quantum efficiency, and efficiency droop of monolayer MoS₂ light-emitting devices,” *Nano Lett.*, vol. 14, pp. 4125–4130, 2014.
- [13] D.-H. Kang, S. R. Pae, J. Shim, et al., “An ultrahigh-performance photodetector based on a perovskite–transition-metal-dichalcogenide hybrid structure,” *Adv. Mater.*, vol. 28, pp. 7799–7806, 2016.
- [14] M. Amani, D.-H. Lien, D. Kiriya, et al., “Near-unity photoluminescence quantum yield in MoS₂,” *Science*, vol. 350, p. 1065, 2015.
- [15] X. Zhang, S. Choi, D. Wang, et al., “Unidirectional doubly enhanced MoS₂ emission via photonic Fano resonances,” *Nano Lett.*, vol. 17, pp. 6715–6720, 2017.
- [16] Z. Li, C. Liu, X. Rong, et al., “Tailoring MoS₂ valley-polarized photoluminescence with super chiral near-field,” *Adv. Mater.*, vol. 30, 2018, Art no. 1801908.
- [17] S. Zu, T. Han, M. Jiang, et al., “Imaging of plasmonic chiral radiative local density of states with cathodoluminescence nanoscopy,” *Nano Lett.*, vol. 19, pp. 775–780, 2019.
- [18] H. Shan, Y. Yu, X. Wang, et al., “Direct observation of ultrafast plasmonic hot electron transfer in the strong coupling regime,” *Light Sci. Appl.*, vol. 8, p. 9, 2019.
- [19] Z. Wang, Z. Dong, Y. Gu, et al., “Giant photoluminescence enhancement in tungsten-diselenide–gold plasmonic hybrid structures,” *Nat. Commun.*, vol. 7, 2016, Art no. 11283.
- [20] S. Zu, B. Li, Y. Gong, et al., “Active control of plasmon–exciton coupling in MoS₂–Ag hybrid nanostructures,” *Adv. Opt. Mater.*, vol. 4, pp. 1463–1469, 2016.
- [21] Z. Li, Y. Xiao, Y. Gong, et al., “Active light control of the MoS₂ monolayer exciton binding energy,” *ACS Nano*, vol. 9, pp. 10158–10164, 2015.
- [22] G. T. Forcherio, M. Benamara, and D. K. Roper, “Electron energy loss spectroscopy of hot electron transport between gold nanoantennas and molybdenum disulfide by plasmon excitation,” *Adv. Opt. Mater.*, vol. 5, 2017, Art no. 1600572.
- [23] W. Gao, Y. H. Lee, R. Jiang, et al., “Localized and continuous tuning of monolayer MoS₂ photoluminescence using a single shape-controlled ag nanoantenna,” *Adv. Mater.*, vol. 28, pp. 701–706, 2016.
- [24] Y. Kang, S. Najmaei, Z. Liu, et al., “Plasmonic hot electron induced structural phase transition in a MoS₂ monolayer,” *Adv. Mater.*, vol. 26, pp. 6467–6471, 2014.
- [25] D. Voiry, A. Goswami, R. Kappera, et al., “Covalent functionalization of monolayered transition metal dichalcogenides by phase engineering,” *Nat. Chem.*, vol. 7, pp. 45–49, 2015.
- [26] A. Yang, J.-C. Blancon, W. Jiang, et al., “Giant enhancement of photoluminescence emission in WS₂-two-dimensional perovskite heterostructures,” *Nano Lett.*, vol. 19, pp. 4852–4860, 2019.
- [27] Y. Liu, H. Li, X. Zheng, et al., “Giant photoluminescence enhancement in monolayer WS₂ by energy transfer from CsPbBr₃ quantum dots,” *Opt. Mater. Express*, vol. 7, p. 1327, 2017.
- [28] J. Gu, B. Chakraborty, M. Khatoniar, et al., “A room-temperature polariton light-emitting diode based on monolayer WS₂,” *Nat. Nanotechnol.*, vol. 14, pp. 1024–1028, 2019.
- [29] L. Qiu, C. Chakraborty, S. Dhara, et al., “Room-temperature valley coherence in a polaritonic system,” *Nat. Commun.*, vol. 10, p. 1513, 2019.
- [30] H. Zeng, J. Dai, W. Yao, et al., “Valley polarization in MoS₂ monolayers by optical pumping,” *Nat. Nanotechnol.*, vol. 7, pp. 490–493, 2012.

- [31] K. F. Mak, K. He, J. Shan, et al., “Control of valley polarization in monolayer MoS₂ by optical helicity,” *Nat. Nanotechnol.*, vol. 7, pp. 494–498, 2012.
- [32] T. Jiang, H. Liu, D. Huang, et al., “Valley and band structure engineering of folded MoS₂ bilayers,” *Nat. Nanotechnol.*, vol. 9, pp. 825–829, 2014.
- [33] B. Zhu, H. Zeng, J. Dai, et al., “Anomalous robust valley polarization and valley coherence in bilayer WS₂,” *Proc. Natl. Acad. Sci. Nat. Nanotechnol.*, vol. 111, 2014, Art no. 11606.
- [34] Y. Wang, C. Cong, J. Shang, et al., “Unveiling exceptionally robust valley contrast in AA- and AB-stacked bilayer WS₂,” *Nanoscale Horiz.*, vol. 4, pp. 396–403, 2019.
- [35] A. Granados del Águila, S. Liu, T. T. H. Do, et al., “Linearly polarized luminescence of atomically thin MoS₂ semiconductor nanocrystals,” *ACS Nano*, vol. 13, pp. 13006–13014, 2019.
- [36] L. Zhang, R. Gogna, W. Burg, et al., “Photonic-crystal exciton-polaritons in monolayer semiconductors,” *Nat. Commun.*, vol. 9, p. 713, 2018.
- [37] A. M. Dibos, Y. Zhou, L. A. Jauregui, et al., “Electrically tunable exciton–plasmon coupling in a WSe₂ monolayer embedded in a plasmonic crystal cavity,” *Nano Lett.*, vol. 19, pp. 3543–3547, 2019.
- [38] Y. Tang, Y. Zhang, H. Ouyang, et al., “Ultrafast response of a hybrid device based on strongly coupled monolayer WS₂ and photonic crystals: the effect of photoinduced coulombic screening,” *Laser Photonics Rev.*, vol. 14, 2020, Art no. 1900419.
- [39] V. Kravtsov, E. Khestanova, F. A. Benimetskiy, et al., “Nonlinear polaritons in a monolayer semiconductor coupled to optical bound states in the continuum,” *Light Sci. Appl.*, vol. 9, p. 56, 2020.
- [40] X. Zhang, C. De-Eknamkul, J. Gu, et al., “Guiding of visible photons at the ångström thickness limit,” *Nat. Nanotechnol.*, vol. 14, pp. 844–850, 2019.
- [41] S. Wu, S. Buckley, A. M. Jones, et al., “Control of two-dimensional excitonic light emission via photonic crystal,” *2D Mater.*, vol. 1, p. 11001, 2014.
- [42] X. Gan, Y. Gao, K. Fai Mak, et al., “Controlling the spontaneous emission rate of monolayer MoS₂ in a photonic crystal nanocavity,” *Appl. Phys. Lett.*, vol. 103, 2013, Art no. 181119.
- [43] S. Wu, S. Buckley, J. R. Schaibley, et al., “Monolayer semiconductor nanocavity lasers with ultralow thresholds,” *Nature*, vol. 520, pp. 69–72, 2015.
- [44] E. Y. Paik, L. Zhang, G. W. Burg, et al., “Interlayer exciton laser of extended spatial coherence in atomically thin heterostructures,” *Nature*, vol. 576, pp. 80–84, 2019.
- [45] W. Liu, B. Wang, Y. Zhang, et al., “Circularly polarized states spawning from bound states in the continuum,” *Phys. Rev. Lett.*, vol. 123, 2019, Art no. 116104.
- [46] J. Wang, H. Li, Y. Ma, et al., *Routers of valley excitons in a WS₂ monolayer via delocalized Bloch modes of in-plane inversion-symmetry broken photonic crystal slabs*, 2020. arXiv:2003.09589.

Supplementary material: The online version of this article offers supplementary material (<https://doi.org/10.1515/nanoph-2020-0294>).